# Microfluidic Multiple Cell Chip Reactor Filled with Enzyme-Coated Magnetic Nanoparticles — An Efficient and Flexible Novel Tool for Enzyme Catalyzed Biotransformations

**Ferenc Ender[1]*, Diána Weiser[2], Botond Nagy[3], Csaba László Bencze[3], Csaba Paizs[3], Péter Pálovics[1] and László Poppe[2,4]***

[1]*Department of Electron Devices, Budapest University of Technology and Economics, Budapest, Magyar tudósok körútja 2., H-1117 Budapest, Hungary*
[2]*Department of Organic Chemistry and Technology, Budapest University of Technology and Economics, Műegyetem rkp. 3., H-1111 Budapest, Hungary*
[3]*Biocatalysis and Biotransformation Research Group, Babeş-Bolyai University of Cluj-Napoca, Arany János str. 11, Ro-400028 Cluj-Napoca, Romania*
[4]*SynBiocat Ltd., H-1173 Budapest, Lázár deák u. 4/1., Hungary*

Received: 14 October 2015; accepted: 02 December 2015

Biotransformation of L-phenylalanine (L-**1a**) and five unnatural substrates (*rac*-**1b**–**f**) by phenylalanine ammonia-lyase (PAL) was investigated in a novel microfluidic device (Magne-Chip) that comprises microliter volume reaction cells filled with PAL-coated magnetic nanoparticles (MNPs). Experiments proved the excellent reproducibility of enzyme-catalyzed biotransformation in the chip and the excellent reusability of the enzyme layer during 14 h continuous measurement (>98% over 7 repetitive measurements with L-**1a**). The platform also enabled fully automatic multi-parameter measurements with a single biocatalyst loading of about 1 mg PAL-MNP. Computational fluid dynamics (CFD) calculations were used to study the flow field in the chambers and the effect of unintended bubble formation. Optimal flow rate for L-**1a** reaction and specific activities for *rac*-**1b**–**f** under these conditions were determined.

**Keywords:** magnetic nanoparticle, magnetic chip reactor, continuous-flow biotransformation, phenylalanine ammonia-lyase, unnatural amino acid

## 1. Introduction

**1.1. Phenylalanine Ammonia-Lyase (PAL).** Phenylalanine ammonia-lyase (PAL; EC 4.3.1.24), catalyzing the nonoxidative deamination of L-phenylalanine (L-**1a**) into (*E*)-cinnamic acid (**2a**), is a member of the aromatic amino acid lyase family [1]. PAL is a key biosynthetic catalyst in phenyl-propanoid assembly in plants and fungi and is involved in the biosynthesis of a wide variety of secondary metabolites such as flavonoids, furanocoumarin phytoalexins, and cell wall components [2]. PAL has potential as therapeutic enzyme in enzyme replacement therapy of humans afflicted with phenylketonuria [3]. PAL was also applied as biocatalyst in the preparation of various aromatic L- and D-α-amino acids of high enantiopurity [1, 4].

**1.2. Magne-Chip Platform.** Microfluidic application of immobilized enzymes [5] offers novel possibilities in diagnostics [6, 7], synthetic [8], or analytical [9, 10] applications. PAL covalently attached to magnetic nanoparticles (MNPs) [11] is applicable as biocatalyst in microfluidic systems in variable ways. PAL-coated MNPs are able to flow in microfluidic systems together with the liquid [6] or can be anchored at predesigned positions of the microreactor by external magnets, thereby enabling a flow of the fluid through the microchannels forming within the anchored MNP layer [7]. This creates a unique opportunity to develop modular micro-systems with the ability of flexible variation of biocatalysts [11].

Magne-Chip is a microfluidic platform that comprises the necessary fluid actuators (e.g., pumps, valves, and thermostat) and sensors (e.g., pressure sensor), a flow controller and a microfluidic chip containing a number of microliter volume reaction chambers. The chambers are addressable selectively by a directed magnetic field, which makes the accumulation of MNPs from a previously selected MNP suspension in the selected chambers possible. In the present paper, the main objective was to study the properties and parameter settings of the Magne-Chip system in biotransformations with PAL using the natural substrate L-phenylalanine (L-**1a**) and five unnatural amino acids (*rac*-**1b**–**f**) including DL-2-amino-3-(4-bromophenyl) propanoic acid (*rac*-**1b**) which has never been tested as substrate for PAL from *Petroselinum crispum* (*Pc*PAL) [1].

* Authors for correspondence: ender@eet.bme.hu (F. Ender), poppe@mail.bme.hu (L. Poppe)

## 2. Results

Reliability and reproducibility of the experiments performed with the Magne-Chip platform (Figure 1) on the natural substrate L-phenylalanine L-**1a** were analyzed experimentally. These tests provided the basis of the in-chip biotransformation study with PAL-coated MNPs (referred as MNPs) acting on unnatural substrates (*rac*-**1b**–**f**, in Scheme 1). First, substrate concentration and flow rate were studied and optimized with L-**1a**. Then biocatalytic activity of the in-chip biotransformation with each unnatural amino acid (*rac*-**1b**–**f**) was determined and compared to the biocatalytic activity of L-phenylalanine L-**1a** as a reference.

**2.1. Performing Multiparameter Experiments in Magne-Chip.** The experiments in Magne-Chip involved four steps: (1) filling up the chip with MNPs, (2) absorbance calibration, (3) experiment cycles, and (4) chip cleaning.

In the chip filling step (see Section 4.3.4 in Experimental), an MNP suspension was driven through the chip by applying a slight air pressure (0.2–0.3 bar) to the vial containing the MNP suspension and connected to the inlet of Magne-Chip via a PTFE tube (Figure 1, "Chip filling") at 25 °C. During the filling process, the MNPs were accumulated in the reaction cells due to the permanent magnets placed in moveable drawers enabling "on/off" switching of the magnetic field. Once the cell most distant from the inlet (Figure 1, Cell #4) was saturated, the magnet of the cell at closer position was turned on (Figure 1, Cell #3). The same procedure was repeated (Figure 1: Cells #2 and #1) until all chambers were filled up. Each cell of the Magne-Chip device could capture ca. 250 μg of MNP biocatalyst [12].

DOI: 10.1556/1846.2015.00036


First published online: 13 February 2016

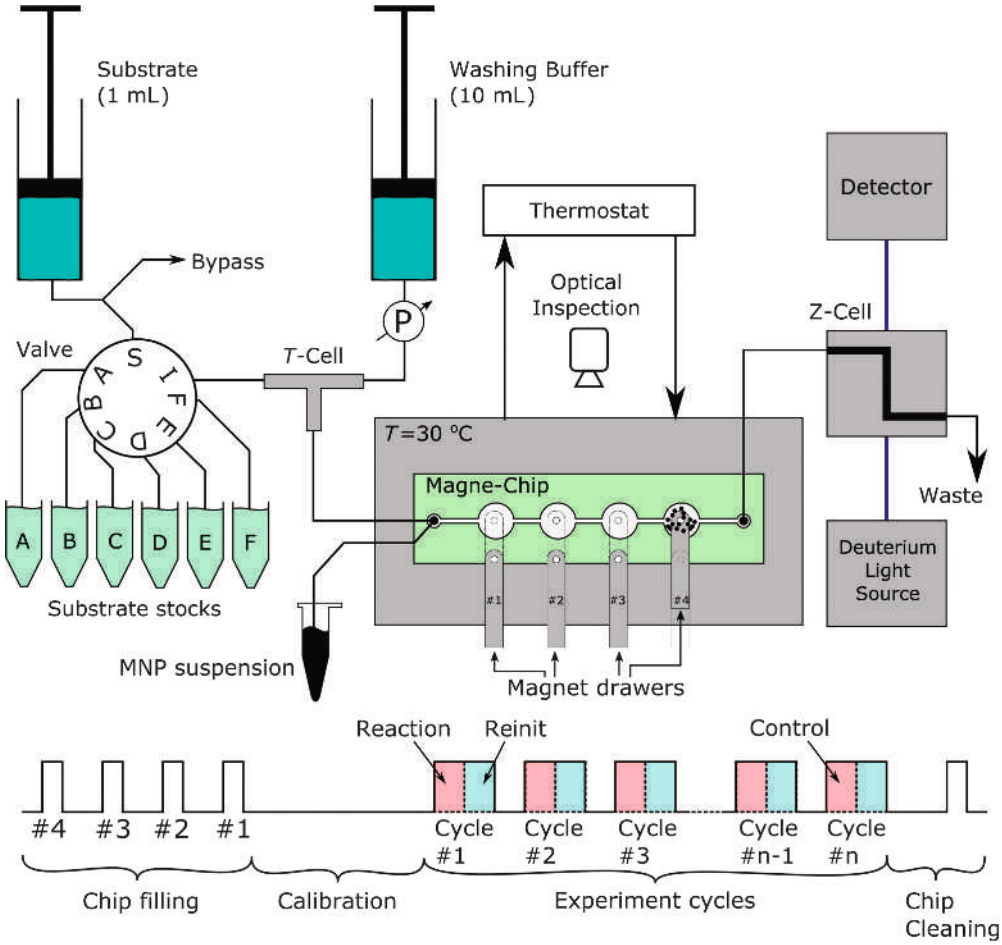


**Figure 1.** Schematic diagram of the fluid control system

During the forthcoming steps (Figure 1, "Calibration," "Experiment cycles"), the valve at the inlet of the Magne-Chip was switched to the substrate (reagent) circuit. The flow controller performed the dosage of the substrate and other chemicals as dictated by the programmed sequence.

At the final chip cleaning step (Figure 1, "Chip cleaning"), the magnetic drawers were drawn out and a washing solution was driven through the chip to remove MNPs.

Each experiment cycle (Figure 1, "Experiment cycles") involves a reaction step and a reinitialization step. A more detailed description of the operation cycle of the chip can be found in Section 4.3.10 of Experimental.

### 2.2. Reliability Assessment of the Measurements

***2.2.1. General Considerations on the Measurements in Magne-Chip.*** As the Magne-Chip system is a quite unexploited tool so far, first the reliability assessment of the measurements was performed. A series of subsequent measurements performed by the system can be considered as reliable if all the following conditions are met:

- the product of the enzyme reaction can be measured selectively in the ultraviolet–visible (UV–vis) range;

**Scheme 1.** Ammonia elimination from different amino acids (**1a**–**f**) catalyzed by *Pc*PAL immobilized onto MNPs

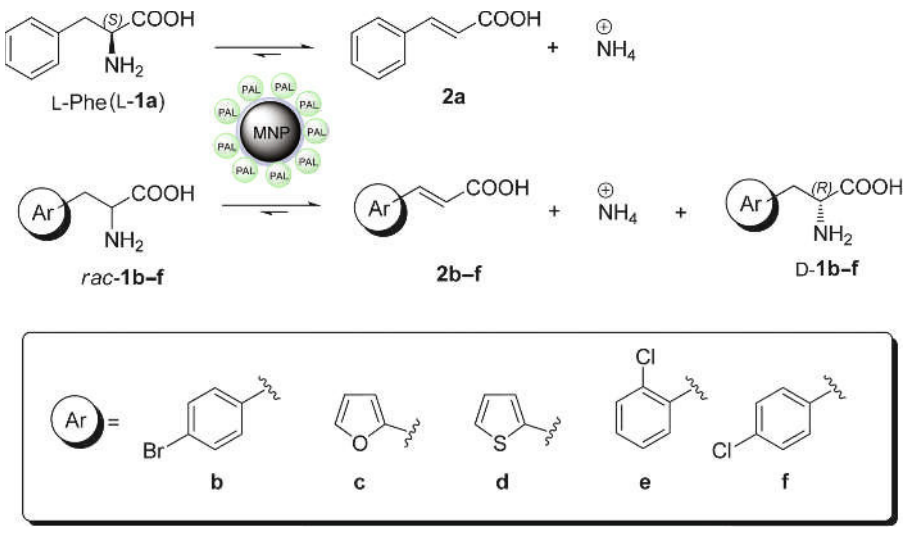

• product and substrate can be completely removed through the washing steps;

• the enzymatic activity of the MNP biocatalyst remains unchanged during the measurement;

• and last but not the least, the MNP layer in the magnetic reactors remain unharmed during the measurement cycles.

In order to test the fulfillment of the first group of conditions, a control measurement was performed after each series of experiments, i.e., the first step of the sequence was repeated in the last step under the same conditions and the specific activity of the immobilized biocatalyst ($U_B$) at saturation concentrations of L-phenylalanine (L-**1a**) in the first and last cycles was compared.

***2.2.2. Optical Inspection of the Reaction Chambers.*** During the experiments, the chip was optically inspected by a zooming microscope and a monochrome high-speed smart camera. Before evaluating the measurement sequence, the plan view of the chip was stored as a reference ($\Pi_{ref}$). At the end of the step $i$ of the measurement sequence, the plan view of the chip was sampled again ($\Pi_{seq,i}$) and it was compared to the reference as follows:

$$\Pi_{diff}(j,k) = \begin{cases} \Pi_{ref}(j,k), & \Pi_{ref}(j,k) - \Pi_{seq,i}(j,k) < 0 \\ 0, & \Pi_{ref}(j,k) - \Pi_{seq,i}(j,k) \geq 0 \end{cases}$$

where ($j$, $k$) is the pixel coordinates of the plan view image; therefore, the changes in accordance to the reference image are indicated by white pixels. The total sum of white pixels is defined as cell difference score (SC) used as a marker for describing the changes of the MNP layer arrangement. Therefore, the changes compared to the image of the first cycle (reference) were indicated by white areas during the consecutive cycles of the measurement.

***2.2.3. CFD Analysis of the Reaction Cell.*** The 3D model of a single reaction cell was analyzed. In a certain fraction of volume, porous cell zone condition was applied to model the space occupied by the MNPs. Pressure drop values were measured at seven different flow rates between 10 μL/min and 80 μL/min with and without MNPs in the chambers resulting in flow specific pressure drop values of 0.086 kPa/μL/min and 0.059 kPa/μL/min, respectively.

As the flow in the channels is laminar, the pressure is proportional to the velocity:

$$\text{grad}\, p = -\mu \mathrm{D} v$$

where $\mu$ is the dynamic viscosity of the fluid, $p$ is the measured pressure, and $v$ is the flow rate at the inlet. $D$ is the viscous resistance of the porous media (MNP layer). Assuming the parameters of water from the software's material database [13], it was found that $R_D = 2.071 \times 10^{10}/m^2$.

CFD results are presented in two relevant cases in Figure 2c and d; in the first case, the nanoparticle layer fully filled in the chamber, while, in the second case, the MNP layer is partially destroyed by the unintended passage of an air bubble.

***2.2.4. Failures of MNP Layers Detected by Visual Inspection.*** The MNP layer in the magnetic reactors can be damaged due to internal drag forces at higher flow rates and due to bubble development during the reaction or due to unintended bubbles from external sources, which may enter the chip during the measurements.

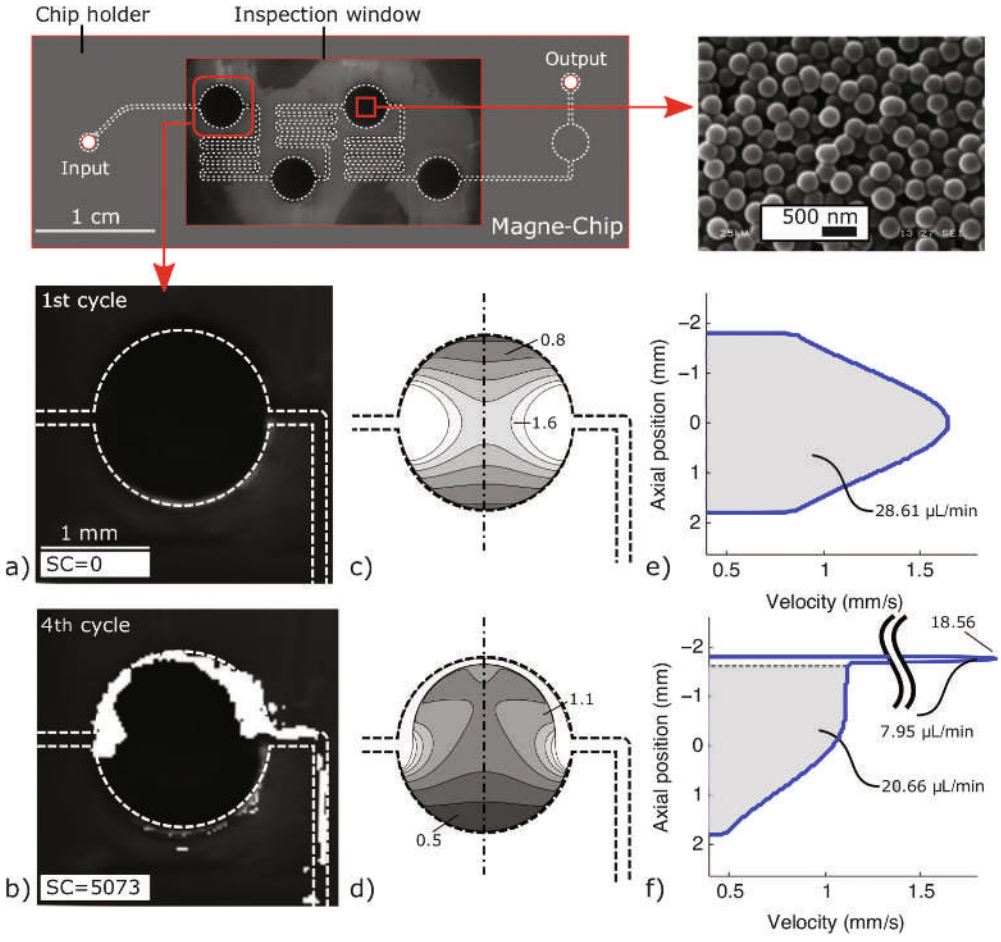


**Figure 2.** Magne-Chip device with four MNP-filled and external magnet-equipped microchambers (top left) and SEM image of the MNP layer (top right). a)–f): The effect of air bubble passage through the reaction cell: a) photograph, before passage; b) difference image (difference score SC= 5073), after passage; c) calculated flow velocity field before and d) after the passage; e) velocity profile in the middle cross section of the chamber before and f) after the passage

Visual inspection of the chambers provides a continuous measure of significant changes (e.g., bubble passage) of the MNP layer structure. Cell difference score (SC) characterizes the actual arrangement of the layer compared to the initial (reference) image. The effect of the air bubble passage can be seen in Figure 2.

In practice, SC values under 2000 usually reflect negligible changes. However, SC >3000 may indicate a serious structural change of the MNP layer, for instance, the complete breakthrough of a bubble (Figure 2b). Air bubbles usually do not split at the channel entrance and rather pass on one side along the chamber wall. While passing through, the bubble elongates; therefore, the middle section of the developed tunnel is narrower (~300 μm). Numerical simulations revealed (Figure 2c, d, e, and f) that the velocity profile became asymmetric due to the bubble passage and the overall mass flow rate through the porous MNP layer significantly decreased (28.6 μL/min to 20.7 μL/min, roughly 72% of its original value) while the remaining fluid passed through the developed tunnel. In the relatively decreased velocity field, the substrate concentration may fall below the saturation level. Additionally, the passing bubble may also drift away particles which decreases the sum mass of biocatalysts. Therefore, the biocatalytic activity of the damaged cell decreased and the consequent measurements were no longer reliable.

***2.2.5. Reliability Assessment of the Measurements.*** Reliability assessment of the measurements was based mostly on the following parameters:

1. Cell difference score (SC) — Over SC >4000 (average), the measurement was declined.

2. Control measurement — Over 5% of error the measurement was declined.

Table 1 summarizes the assessment evaluation of the measurements.

**2.3. Reproducibility of the Individual Measurements**

***2.3.1. Suspension Homogeneity and the Effect of Filling the Chambers with MNP.*** Biotransformation of L-phenylalanine (L-**1a**) to (*E*)-cinnamic acid (**2a**) by MNP biocatalyst suspension (Scheme 1) was performed in *s*hake vial as three parallel reactions and resulted in $U_B$=2.91±0.08 μmol/g/min (for working conditions, see Section 4.3.10, Table 4 in Experimental) ensuring that the homogeneity of the MNP suspension was sufficient.

The first single chamber of the Magne-Chip was filled with MNP suspension. Biotransformation of (L-**1a**) to (**2a**) was performed in flow-through mode and monitored by on-line UV–vis. After reaching the stationary state (i.e., constant level of product formation), the magnet of the chamber was released and the MNPs were captured in the next chamber. The experiments performed in three consecutive chambers were repeated three times resulting in $U_B$ = 8.01 ± 0.14 μmol/g/min.

The filling–refilling results indicated that neither the homogeneity of the MNP suspension nor the filling procedure of the chambers had remarkable effect on the reproducibility of the measurements. The significant difference between the $U_B$ values of MNP biocatalyst in shake vials and in Magne-Chip indicated increased effectivity of the biocatalysts in Magne-Chip device. The volumetric productivity of the ammonia elimination of L-**1a** catalyzed by the MNP biocatalyst was compared in the Magne-Chip and in shake vials indicating more than three orders of magnitude higher value in Magne-Chip (8.82 g/L/h) than that in the shake vial ($3.13\times10^{-3}$ g/L/h).

***2.3.2. Reinitialization of the Chip and Reuse of the MNP Biocatalyst in Cyclic Measurements.*** Magne-Chip was filled with MNP biocatalyst, and biotransformation of L-**1a** to **2a** was performed in 7 consecutive cycles (for working conditions, see Section 4.3.10, Table 4 in Experimental), while the chip was reinitialized during the steps by washing out the substrate and product completely. The absorbance plot in Figure 3 shows the concentration change of **2a** at the specific wavelength of 290 nm. It can be clearly seen that the chip was successfully reinitialized in every cycle throughout the experiment and the reaction was repeated seven times, reaching the same level of conversion. The product quantity was calculated in each cycle.

Two independent experiments are shown in Figure 4. In the first attempt (Figure 4, blue bars), the MNP layer remained stable throughout the measurement, resulting in an average product quantity of $P$=0.12±1.5% μmol. The moderate mean value of the cell difference score SC=1322 (1609 max) also reflects negligible changes in the MNP layer. However, the significantly higher mean SC=4158 (5742 max) in the second attempt (Figure 4, red bars) indicated a damaged MNP layer structure due to air bubble passage. It was also remarkable that the cyclic product quantity decreased abruptly as the SC value elevated above the critical value. In fact, the air bubble, previously stalled (3rd cycle) in the reaction cell, finally drifted away leaving a tunnel behind in the 4th cycle (Figure 2b).

The above results indicated the excellent reproducibility of the reactions in a periodical sequence within the chip when the MNP layer remained undamaged.

**2.4. Influence of the Flow Rate on Biotransformation with L-1a.** Magne-Chip was filled with MNP biocatalyst and biotransformations of L-**1a** to **2a** at various flow rates were performed in 7 consecutive cycles, while the chip was reinitialized at the end of each cycle and a new substrate flow rate was set (for working conditions, see Section 4.3.10, Table 4 in Experimental). The lowest flow rate was set to 3.6 μL/min and increased in the forthcoming steps up to 28.6 μL/min (Figure 5). The first (reference) measurement was repeated in the last cycle as a control. The

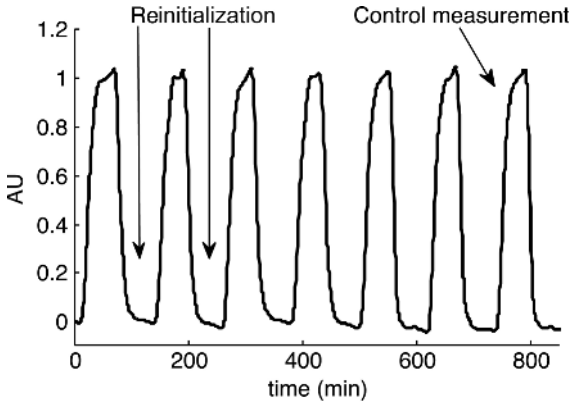


**Figure 3.** Time plot of the periodic absorbance change during the cyclic measurement (attempt 1, stable layer). The chip is reinitialized between the reaction steps (reaching zero absorbance) by washing out substrate and product completely. The last measurement served as a control

**Table 1.** Summary of reliability assessment measures

| Experiment | Error of the control measurement[a] (%) | SC average | SC maximum | Assessment |
|---|---|---|---|---|
| Multiple fillings, MNP load | 3.1 | – | – | Accepted |
| Single parameter, cyclic (attempt 1) | 1.4 | 1322 | 1609 | Accepted |
| Single parameter, cyclic (attempt 2) | 32.0 | 4158 | 5742 | Declined |
| Flow rate optimization | 3.2 | 196 | 338 | Accepted |
| Substrate screening | 1.5 | 1691 | 2000 | Accepted |

[a] Calculation is based on the ratio of the saturation $U_B$ values of the first and last (control) measurement.

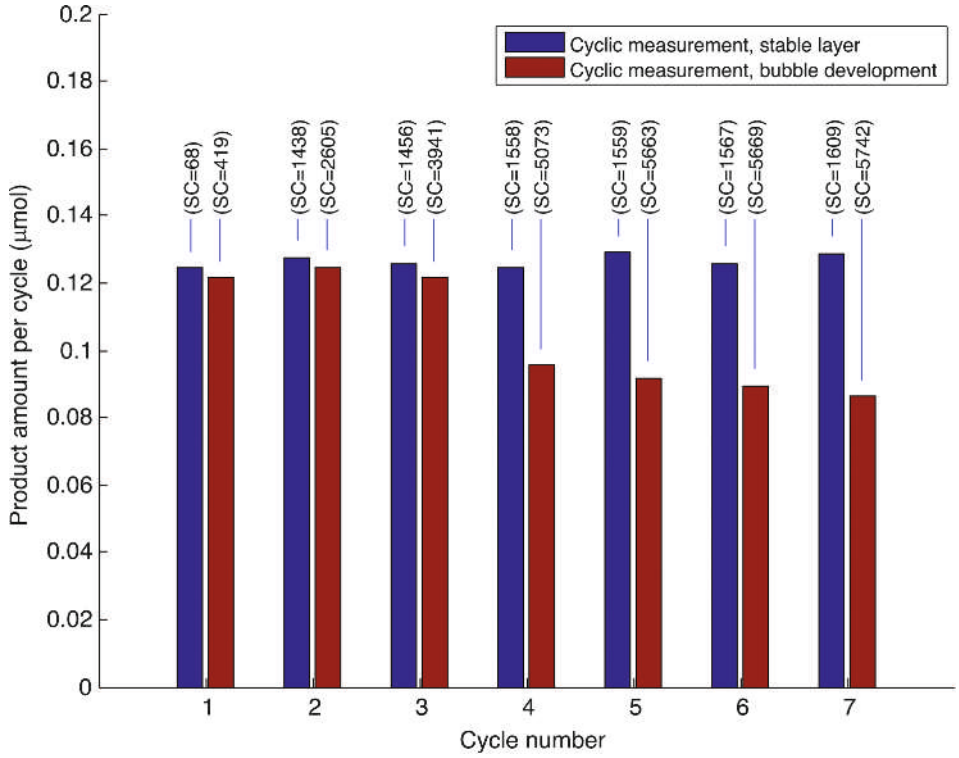


**Figure 4.** Product amount *P* per reaction cycle during a cyclic measurement with unmodified parameter settings. Blue bars indicate the attempt with unharmed MNP layer (SC <2000) with excellent reproducibility while air bubble passage damaged the layer (SC >4000) during the second attempt and demolished the biocatalytic activity (red bars)

negligible difference of specific biocatalytic activity ($U_B$) between the reference and control measurements (only 3%) indicated that the shear forces did not cause irreversible changes on the biocatalytic activity even at high flow rate (up to 28.6 µL/min).

The reaction velocity was calculated for each cycle (for details, see Section 4.3.11 in Experimental). By increasing the flow rate, the calculated reaction velocity increased until reaching saturation at about 25 µL/min.

The uneven flow velocity field inside the reaction cells (Figure 2c) implies that the central section of the chamber reached the saturation velocity even at lower flow rates while, at roughly 25 µL/min inlet flow rate, all the biocatalysts in the whole area of the chamber turned into saturation.

**2.5. Finding the Saturation Substrate Concentration of L-1a.** Magne-Chip was filled with MNP biocatalyst, and biotransformations of L-**1a** to **2a** at various concentrations of L-**1a** [$S_0$] were performed in 10 consecutive cycles, while the chip was reinitialized at the end of each cycle and a new substrate concentration was set (Figure 6, top; for working conditions, see Section 4.3.10, Table 4 in Experimental). It was found that the reaction followed the first order kinetics up to [$S_0$]=3 mM and saturated roughly at [$S_0$]=20 mM.

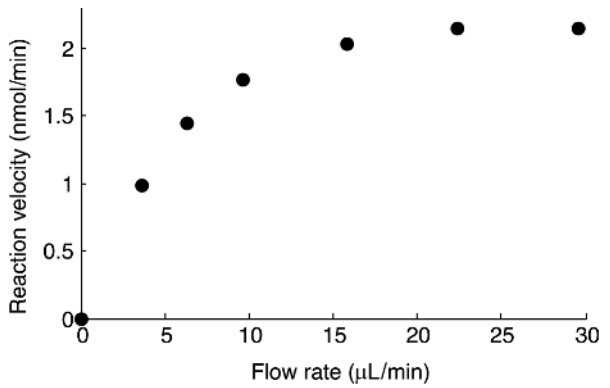


**Figure 5.** Dependence of the reaction rate of L-**1a** conversion to **2a** on the flow rate in Magne-Chip filled by MNP-PAL. Saturation was reached at 25 µL/min

The linear fitting method proposed by Lilly, et al. [14] was applied for the calculation of the kinetic constants of the biotransformation of L-**1a** to **2a** (Figure 6, bottom). The values of the kinetic constants are summarized in Table 2. It was found that the apparent $K_m$ value was reasonably smaller in Magne-Chip (2.5 mM) than in shake vial (9.1 mM). Turnover number ($k_{cat}$) and specificity constant ($k_{cat}/K_m$) were determined also for both reaction modes. While in the shake vial, the turnover number was somewhat higher ($3.2 \cdot 10^{-2}$/s) than the in chip ($2.8 \cdot 10^{-2}$/s), the specificity constant turned out to be significantly higher in chip (11.3/s/M) as compared to the shake vial (3.5/s/M). This may be attributed to the smaller $K_m$ value in the Magne-Chip indicating significant contribution of diffusion effects to the higher apparent $K_m$ value in shake vial.

**2.6. Substrate Screening with MNP Biocatalyst in the Magne-Chip System.** The screening experiments were performed with the natural substrate (L-**1a**), four different phenylalanine analogues as known substrates of *Pc*PAL (*rac*-**1c**–**f**), and 4-bromophenylalanine (*rac*-**1b**) which has never been tested as substrate for *Pc*PAL (cf. Scheme 1). For the substrate screening, the same stock of MNP biocatalyst was used as for the previous experiments (Sections 2.2–2.5).

First, the extinction coefficients of the corresponding elimination products (**2a**–**f**, cf. Scheme 1) were determined at selected wavelengths (Figure 7: preferably at wavelengths resulting in high absorbance of the acrylic acid **2** while practically zero of the amino acid **1a**–**f**) using the flow-cell spectrometer of the Magne-Chip platform. The extinction coefficients at the selected wavelengths were calculated from the quite well fitting linear regressions for dependence of absorbance on molar concentration in each case (Table 3).

The substrate screening experiments were performed with a single chip loading mode passing the solutions of the different substrates (L-**1a** and *rac*-**1b**–**f**) through the chip according to a

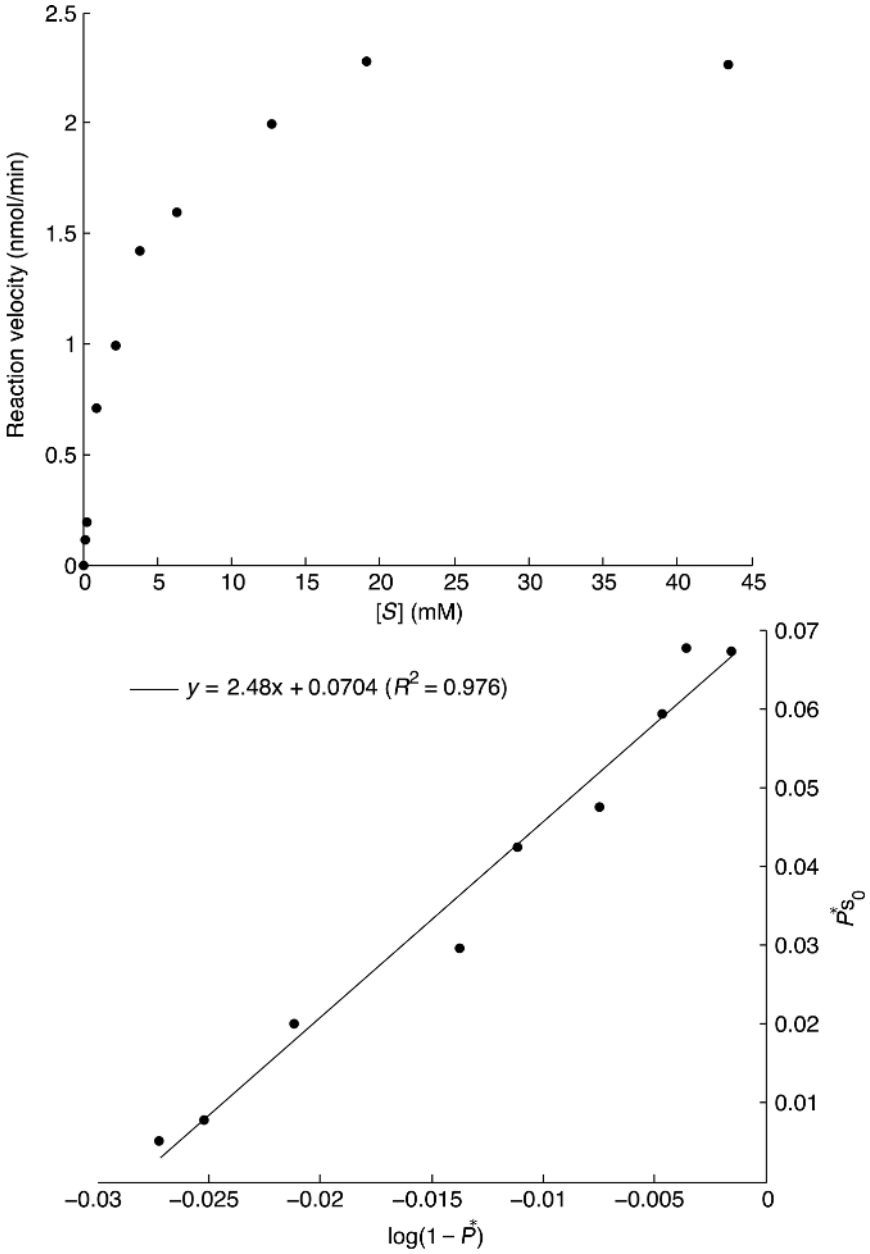


**Figure 6.** Top: Dependency of the substrate concentration on reaction velocity in Magne-Chip for the transformation of L-**1a** to **2a** by MNP biocatalyst. Saturation concentration was reached at 20 mM. Bottom: Linear fit based on the Lilly–Hornby model [14] to determine $K_m$ (resulting in $K_m$=2.5 mM)

**Table 2.** Kinetic constants in biotransformation of L-**1a** to **2a** with MNP in shake vial and in Magne-Chip

| Kinetic parameter | Magne-Chip | Shake vial |
|---|---|---|
| $K_m$ (mM) | 2.5 | 9.1 |
| $k_{cat}$ (/s) | $2.8 \cdot 10^{-2}$ | $3.2 \cdot 10^{-2}$ |
| $k_{cat}/K_m$ (/s/M) | 11.3 | 3.5 |

predefined sequence. The intensive washing procedure ensured complete removal of any substrate or product from the preceding cycle (reaction). In the first cycle, the ammonia elimination was measured from L-**1a** (the natural substrate of PAL). This reaction was chosen as reference for comparison to the other elimination reactions of PAL from the further substrates (*rac*-**1b**–**f**). Surprisingly, in the Magne-Chip device, higher biocatalytic activities ($U_B$) were observed for four of the unnatural substrates (*rac*-**1b**,**c**,**e**,**f**) than for the natural substrate L-phenylalanine L-**1a** (Figure 8).

Noteworthy, all the four unnatural substrates (*rac*-**1b**,**c**,**e**,**f**) which were transformed by the MNP biocatalyst with higher specific biocatalytic activity ($U_B$) than that of L-phenylalanine L-**1a** contained slightly more electron-withdrawing aromatic moieties than the phenyl group. This difference from the productivity ranks observed with homogenous *Pc*PAL so far [1] may be due to the reduced contribution of the reverse reaction (equilibrium effect) to the apparent forward reaction rates in the continuous-flow system at high flow rates.

## 3. Conclusion

A microfluidic device, which consisted four microliter volume reaction chambers filled with *Pc*PAL-coated magnetic nanoparticles (MNP) as functional biocatalyst, was characterized. In the chambers of the chip, MNPs could be captured or released with the aid of moveable external permanent magnets. The microfluidic device could be operated cyclically.

The filling procedure as well as the reactions in the chambers was found highly reproducible (1.5% variation around the mean within cyclic operations of a 14-h timeframe, if no MNP layer-degradation happened).

Saturation flow rate and substrate concentration of the in-chip deamination of L-phenylalanine L-**1a** to (*E*)-cinnamic acid **2a** were found to be 25 μL/min and 20 mM, respectively.

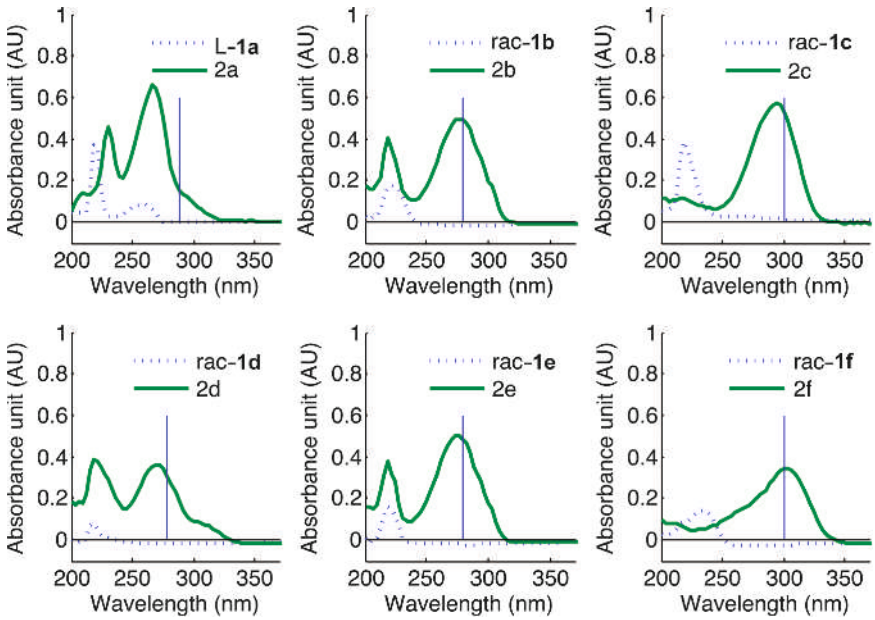


**Figure 7.** UV absorbance spectra of L-**1a** and *rac*-**1b**–**f** (green lines) and the corresponding acrylic acids **2a**–**f** (dotted purple lines). The wavelengths chosen to determine the extinction coefficients are indicated by blue markers

**Table 3.** Extinction coefficients of acrylic acids **2a**–**f**

| Acrylic acid | Wavelength (nm) | Extinction coefficient (/M/cm) | Linear regression coefficient |
|---|---|---|---|
| **2a** | 290 | 8800 | 0.991 |
| **2b** | 300 | 10200 | 0.998 |
| **2c** | 300 | 7919 | 0.988 |
| **2d** | 280 | 14721 | 0.993 |
| **2e** | 280 | 9172 | 0.991 |
| **2f** | 280 | 15327 | 0.998 |

The Magne-Chip system equipped with an on-line UV–vis flow cell could be applied for automated activity screening of four known (*rac*-**1c**–**f**) and a novel (*rac*-**1b**) unnatural substrate of *Pc*PAL compared to the natural substrate L-**1a** by a cyclic test series using the same MNP filling. The specific biocatalytic activity of MNP with five unnatural substrates (*rac*-**1b**,**c**,**e**,**f**) exceeded that of with the natural substrate (L-**1a**), unlike in the corresponding reactions with native *Pc*PAL where only the thiophen-2-yl derivative *rac*-**1d** had higher specific activity.

Our results proved that the Magne-Chip microfluidic device is a reliable, reproducible, and efficient tool which was capable of fast, reliable, and fully automated screening of *Pc*PAL substrates using minimal solvent (~500 μL) and biocatalyst (~1 mg MNP) amounts for a test compound. Compared to shake vial, the volumetric productivity of the MNP biocatalyst in the chip exceeded one of the shake vial by more than three orders of magnitude.

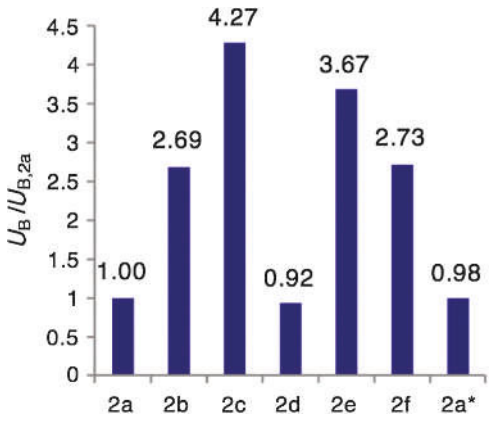


**Figure 8.** Comparison of the specific biocatalytic activity of *Pc*PAL immobilized on MNPs with substrates L-**1a** and *rac*-**1b**–**f** in Magne-Chip system ([*S*]=20 mM, flow rate: 48.6 μL/min). *Control measurement

## 4. Experimental

### 4.1. Materials

***4.1.1. Phenylalanine Ammonia-Lyase from Parsley (P. Crispum).*** Phenylalanine ammonia-lyase (PAL) from parsley (*P. crispum*) was overexpressed in *Escherichia coli* and purified according to the method described by Poppe et al. [1].

***4.1.2. Chemicals.*** Functionalized magnetic nanoparticles for covalent binding of PAL (MagneCat-250GP14) were obtained from SynBiocat LLC (Budapest, Hungary). Detergent EMAG EM-080 was obtained from EMAG AG (Mörfelden-Walldor, Germany). L-Phenylalanine, cinnamic acid, tris(hydroxymethyl) aminomethane (TRIS), polyethylene glycol 4000 (PEG 4000), 2-propanol, DL-2-amino-3-(4-bromophenyl)-propanoic acid (*rac*-**1b**), and (*E*)-3-(4-bromophen*y*l)acrylic acid (**2b**) were purchased from Sigma-Aldrich (St. Luis, MO, USA). DL-2-amino-3-(furan-2-yl)propanoic acid (*rac*-**1c**), DL-2-amino-3-(thiophen-2-yl) propanoic acid (*rac*-**1d**), DL-2-amino-3-(2-chlorophenyl)propanoic acid (*rac*-**1e**), DL-2-amino-3-(4-chlorophenyl)propanoic acid (*rac*-**1f**), (*E*)-3-(furan-**2**-yl)*a*crylic acid (**2c**), (*E*)-3-(2-chlorophe*n*yl)acrylic acid (**2e**), (*E*)-3-(thiophen-2-*y*l)acrylic acid (**2d**), and (*E*)-3-(4-chlorophe*n*yl)acrylic acid (**2f**) were synthetized as previously described [15–17].

### 4.2. Equipment

***4.2.1. Microfluidic System with Four Magnetic Microreactor Cells (Magne-Chip).*** The tests were performed in the magnetic-nanoparticle reactor microchip, consisting of four chambers, volume of 1.1 μL each. The chips were made of polydimethyl-siloxane (PDMS, Sylgard 184, Dow Corning Ltd, Germany). PDMS body was bonded onto a glass substrate after plasma treatment. Microchannel dimensions are width of 300 μm and height of 110 μm; reaction cell dimensions are volume of 1.1 μL, diameter of 3.6 mm, and height of 110 μm [12].

The chip was fixed in a microfluidic chip holder (Fluidic Connect Pro, Micronit Inc., The Netherlands). The microfluidic test bench consisted of two precision syringe pumps, stereo zoom microscope with digital camera, deuterium-halogen light source, spectrometer, Z-flow absorbance cell (see details in Section 4.3.1), circulating thermostat (Julabo Inc. type F-25)

and a system controller unit. Gage pressure was measured by MPX4250 (Freescale Semiconductors Ltd., Austin, Texas, US) pressure sensor mounted on the Luer-connector of the syringe (see Figure 1). The system was operated by the μFLU Studio software (developed for the Magne-Chip platform), which controlled the pumps, valves, and the thermostat, acquired the data of the chip sensors (e.g., inlet pressure), inspected the camera picture of the chip, and collected the data of the spectrometer based on the predefined measurement sequence script of the subsequent cases.

**4.3. Methods**

***4.3.1. UV–Vis Measurements.*** UV spectra of L-**1a**, *rac*-1**b**–**f** and the corresponding acrylic acids (**2a**–**f**) were measured by the flow-cell spectrometer setup (deuterium-halogen light source DT-Mini 2GS, spectrometer USB 2000+, Ocean Optics Ltd., USA, Z-flow absorbance cell, Avantes Inc., The Netherlands) in continuous-flow mode (48 μL/min). Absorbance spectra were taken (Figure 8) using the spectrum of the TRIS solution (0.1 M, pH 8.8) as reference.

For the reactions carried out in shake vial, the product content of the supernatants was determined at $\lambda$=290 nm and 30 °C by UV–vis spectrophotometer (Genesys 2, Milton Roy Inc., USA).

***4.3.2. Immobilization PcPAL onto MNPs.*** Epoxy-MNPs (MagneCat-250GP14 [epoxy-functionalized magnetic nanoparticles with an average diameter of 250 nm]: 108 mg) were added to TRIS buffer (3 mL, 0.1 M, pH 8.8) and dispersed by ultrasonication (35 kHz, 20 min). The MNP suspension was added to the *Pc*PAL solution (3 mg/mL, in TRIS buffer: 4 mL, 0.1 M, pH 8.8), and the mixture was shaken for 24 h (25 °C, 450 rpm). The PAL-coated MNP particles were fixed at the bottom of the flask with a neodymium magnet, and the supernatant was decanted. The MNP preparation was washed — by a resuspension – magnetic fixing – decantation sequence in each washing steps — with TRIS buffer (3×4 mL, 0.1 M, pH 8.8) and with ethanol (4 mL). The MNP biocatalyst was dried in vacuum at room temperature for 2 h. After immobilization, negligible protein contents in the supernatants of the washing procedure were determined by the Bradford assay [18].

***4.3.3. Enzymatic Reactions in Shake Vial.*** To determine the kinetic constants of *Pc*PAL immobilized on magnetic nanoparticles, sufficient amount of MNPs (10 mg) was added to the solution of L-**1a** in TRIS buffer (2 mL, 0.1 M, pH 8.8; various concentrations of the substrate L-**1a**) and the mixture was shaken (450 rpm, 30 °C). At each 5 min in a 30-min reaction period, the immobilized biocatalyst was magnetically isolated and the product concentration (**2a**) of the supernatant was determined at $\lambda$=290 nm and 30 °C by UV–vis spectrophotometer. To determine kinetic data, the difference values of the product concentrations between 15 and 20 min were applied.

The specific biocatalytic activity of MNP biocatalyst in shake vials was tested in the ammonia elimination of L-**1a** in nine parallel trials. To ensure full homogeneity, MNP biocatalyst (2.0 mg) and PEG 4000 (2.0 mg) were suspended in TRIS buffer (1 mL, 0.1 M, pH 8.8) by sonication for 30 min. In each test reaction, 500 μL of the above MNP suspension was added to a solution of L-**1a** (500 μL, 40 mM in TRIS buffer; 0.1 M, pH 8.8), and the mixtures were shaken in an Eppendorf thermoshaker (at 850 rpm, 30 °C) for 20 min. MNPs were collected with a permanent neodymium magnet; then the product (**2a**) concentration of the supernatants was determined by UV–vis spectrophotometry at $\lambda$=290 nm and 30 °C.

***4.3.4. Filling of the Magne-Chip Microreactors with MNPs.*** In an Eppendorf tube, a suspension (total volume: 1.5 mL) was prepared from the MNP biocatalyst (3.3 mg/mL) and PEG-4000 (3.3 mg/mL) in a 5:1 mixture of ultrapure water and 2-propanol. The mixture was sonicated for 15 min in an ultrasonic bath (EMAG EMMI 15HC) kept on 30 °C. Right before the filling up process, the suspension was sonicated again for 10 min. During the filling process, the chip was kept on 25 °C. To avoid sedimentation, gentle shaking (700 rpm) was maintained by an orbital shaker (4.5 mm of orbital diameter) during the chip loading procedure. Neodymium magnets (type N48, 3×4 mm) were placed in moveable drawers enabling "on/off" switching of the magnetic field when placed directly below the magnetic cells.

For the optical inspection of the chip, the NI-1772 (National Instruments, USA) smart camera was used mounted to a stereo zoom microscope (10× magnification).

***4.3.5. Cleaning the Chip.*** Detergent solution (1:99 mixture of EMAG EM-080 and ultrapure water) was used for the cleaning of microchannels. At the end of the reaction, by positioning the moveable drawers to "off" position, the magnetic field is deactivated, and TRIS buffer (0.1 M, pH 8.8), solution of detergent, and, finally, ultrapure water were driven through the chip, each for 2 min at 300 μL/min flow rate while the particles were flushed out completely.

***4.3.6. Multiparameter Reactions in Magne-Chip.*** Once the Magne-Chip was filled with MNPs, the dosage of liquids flowing through the chip could be controlled in a programmed manner. As the MNP biocatalysts are reusable, the chip could be cyclically reinitialized by washing after each biotransformation experiment. This enabled the changing of the substrate or modifying the working parameters cycle by cycle without changing the biocatalyst in the system, i.e., screening conditions or various substrates following an automated sequence. Note that the parameter settings of the cycles were stored in a sequence file and the settings had been done automatically by the controller software and hardware.

***4.3.7. Calibration.*** Washing buffer was driven through the chip and the Z-cell (Figure 1) at 440 μL/min flow rate. Once the flow conditions were stable (i.e., no air bubbles in the Z-cell), the total intensity spectra and the dark spectra were stored as references and the calculated absorbance spectra were stored for the total available wavelength range (200–1100 nm) in every second (i.e., the sampling rate was 1 Hz).

***4.3.8. Fluid Handling during the Experiment Cycles.*** One syringe (the "substrate syringe") was filled up through the switching valve (Figure 1, S-A, S-B, … S-F positions) by the adequate substrate from the substrate stocks A–F in accordance to the programmed measurement sequence. Once the substrate syringe (1 mL of volume) was fully loaded, the valve switched to S-I position. Washing buffer was loaded into the other syringe (the "washing buffer syringe"). Substrate, washing buffer, or a mixture of them (mixing ratio is variable from 1:1 to 1:1600) was driven through the chip at a determined flow rate. The internal pressure of the fluid circuitry was continuously monitored through the connector of the "washing buffer syringe." The chip was kept on a predefined temperature through the measurement.

***4.3.9. Experiment Cycles.*** Within a series of experiments (Figure 1, "Experiment cycles"), a single cycle involves a reaction step and a reinitialization step (Figure 9).

*4.3.9.1. Reaction Step (Figure 9, $t_{start,n} - t_{end}$)* The dosage of the substrate began according to one of the following variants (see Section 4.3.10 in Experimental, Table 4, Parameter change). The absorbance value at a previously selected wavelength was continuously monitored. The cycle step ended when the designated step time had been passed or when the reaction had been saturated at least for $\Delta t_{sat,min}$ = 10 min (i.e., absorbance changes fall into the 5% range of the saturation absorbance level), whichever happened earlier.

Variant a) The dosage of the substrate started (1st cycle) or continued at unchanged flow rate.

Variant b) The dosage of the substrate started (1st cycle) or continued while the flow rate may change cycle by cycle.

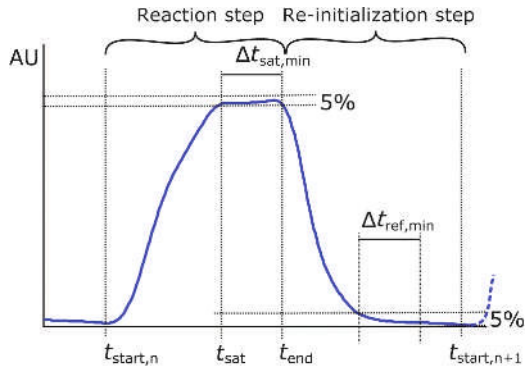


**Figure 9.** Typical absorbance plot over time at a given wavelength for a single cycle of a series of experiments in-chip. Time markers show the integration limits of kinetic calculations. Absorbance markers show the 5% acceptance range of stationary product concentration

Variant c) The dosage of the substrate and the washing buffer ran parallel on a designated ratio resulted in a predefined dilution of the substrate at the chip inlet. The dilution ratio may be different cycle by cycle.

Variant d) The remaining substrate was drained through a bypass valve (Figure 1). The consequent substrate from the substrate stock (A-F) was loaded into the substrate syringe and the dosage of the substrate began at a predefined flow rate.

*4.3.9.2. Reinitialization Step (Figure 9, $t_{end} - t_{start,n+1}$).* The dosage of the substrate stopped while the washing buffer was driven through the system at a designated flow rate. The step ended when the designated step time had been passed or when the absorbance value reached the reference value (i.e., absorbance changes fall into the 5% range of the reference absorbance level) at least for $\Delta t_{ref,min}$=10 min, whichever happened earlier.

A reaction and a reinitialization step constitute one cycle. Cycles are repeated several times (see Section 4.3.10 in Experimental: Table 4, no. of cycles) according to the predefined measurement sequence.

***4.3.10. Enzymatic Reactions in Magne-Chip.*** Table 4 summarizes the settings of the Magne-Chip platform which were applied during the experiments.

***4.3.11. Calculation of Kinetic Parameters in the Magne-Chip.*** Product concentration was calculated by taking the integral of the time-dependent absorbance plot at the product specific wavelength:

$$[P] = \frac{1}{\varepsilon \Delta t} \int_{t_{start}}^{t_{end}} A(t)dt$$

where $[P]$ is the product concentration, $A$ is the absorbance, $\varepsilon$ is the molar extinction coefficient, and $\Delta t$ is the difference of the integration limits.

Product quantity was calculated from the product concentration:

$$P = [P]\dot{Q}\Delta t$$

where $P$ is the product quantity and $\dot{Q}$ is the inlet flow rate.

Specific biocatalytic activity was calculated by taking the integral of the saturation region of the absorbance plot:

$$U_B = \frac{\frac{1}{\varepsilon}\int_{t_{end}}^{t_{sat}} A(t)dt\dot{Q}}{m\Delta t}$$

where $U_B$ is the specific biocatalytic activity and $m$ is the total mass of the MNP biocatalyst.

Reaction velocity ($v$) was defined as:

$$\nu = \frac{P}{\Delta t}.$$

Volumetric productivity ($P_V$) was defined as:

$$P_V = \frac{MP}{V_v \Delta t}$$

where $M$ is the molar mass, $V_v$ is the void volume of the reaction chambers. While the sum volume of the reaction chambers is $V_s$, the void fraction of the chambers is defined as:

$$\beta = \frac{V_v}{V_s}.$$

The insoluble enzyme constituting a filled reactor may be considered as a suspension of enzyme protein in a volume equal to the total volume of the microreactor. Thus:

$$[E] = \frac{E}{V_v}$$

where $E$ is the total amount of enzyme in moles. Let $P^*$ be the fraction of substrate reacted in the reactor volume:

$$P^* = \frac{[S_0 - S_t]}{[S_0]}$$

where $[S_0]$ and $[S_t]$ are the initial substrate concentration and substrate concentration after the residence time of the substrate solution in the chip.

**Table 4.** Summary of the measurement settings

| Experiment | Substrate stocks[a] | Parameter change | Substrate flow rate (μL/min) | Washing flow rate (μL/min) | No. of cycles[b] | MNP mass[c] (mg) |
|---|---|---|---|---|---|---|
| Multiple filling of MNP load | **A** – L-**1a** | Const. [Var. a)] | 48.6 (for 10 min) | 440 (for 5 min) | 4 (in 1 h) | 0.25 (in 1 cell) |
| Single filling, single parameter | **A** – L-**1a** | Const. [Var. a)] | 28.6 (for 1 h) | 28.6 (for 1 h) | 7 (in 14 h) | 1 (in 4 cells) |
| Flow rate optimization | **A** – L-**1a** | Flow rate: 3.6–28.6 μL/min [Var b)] | Varied | 28.6 (for 30 min) | 7 (in 7 h) | 1 (in 4 cells) |
| Reaction saturation | A – L-**1a** 3.3 mM<br>B – L-**1a** 65 mM | [S]: 0.19– 43.4 mM [Var c)] | 28.6 (for 30 min) | 28.6 (for 30 min) | 10 (in 7 h) | 1 (in 4 cells) |
| Substrate screening | **A** – L-**1a**<br>B – *rac*-**1b**<br>C – *rac*-**1c**<br>D – *rac*-**1d**<br>E – *rac*-**1e**<br>F – *rac*-**1f** | Substrate [Var d)] | 48.6 (for 10 min) | 440 (for 10 min) | 7 (in 2.3 h) | 0.5 (in 2 cells) |

[a] When otherwise not stated concentration of substrate was 20 mM. Control measurement in the last cycle was done by the substrate indicated with bold.
[b] One cycle constituted Reaction and Reinitialization steps.
[c] Biocatalyst mass was determined as described earlier.

According to Lilly et al. [14], the kinetics of an insoluble enzyme constituting filled reactor is the following:

$$P[S_0] = K_m \log(1-P^*) + R/\dot{Q}$$

where $R$ is the reaction capacity of the reactor, defined as:

$$R = \mathrm{k_{cat}} E \beta.$$

Here $k_{cat}$ is the turnover number. Based on previous measurements [12], the volume fraction of the particles in the chip can be estimated to be about 7%.

$P^*[S_0]$ plotted against $\log(1-P^*)$ will give a straight line. The slope of the line will be equal to $K_m$ and the intercept on the $P^*[S_0]$ axis will be equal to $R/\dot{Q}$ [14].

**4.4. Numerical Methods.** The velocity distribution of the reaction cell structure was investigated by numerical methods in ANSYS Fluent [13]. Stationary simulation was performed for a three-dimensional pressure-based laminar flow problem with absolute velocity formulation. Velocity inlet was set up for the channel inlet while outflow boundary for the outlet. The SIMPLE simulation method was applied with Least-Squares Cell-Based gradient, Second Order Pressure, and Second Order Upwind Momentum calculations. The inlet velocity condition was set to 28.6 μL/min.

**Acknowledgements.** The authors thank the support from COST Action CM1303 (SysBiocat). L.P. thanks the financial support from Hungarian OTKA Foundation (NN-103242), from the Hungarian Research and Technology Innovation Fund (KMR 12-1-2012-0140), and from the New Hungary Development Plan (TÁMOP-4.2.1/B-09/1/KMR-2010-0002). The financial support provided by the Collegium Talentum Research Program to N.B. and L.P. is also acknowledged. C.P. thanks the financial support from the Romanian National Authority for Scientific Research, CNCS — UEFISCDI (PN-II-IDPCE-2011-3-0799). L.C.B. and N.B. thank the financial support from the Sectoral Operational Program for Human Resources Development 2007–2013, cofinanced by the European Social Fund (projects POSDRU/159/1.5/S/137750 and POSDRU/159/1.5/S/132400).

**Table of Symbols and Units**

| Symbol | | Units |
|---|---|---|
| AU | Absorbance unit | – |
| $E$ | Enzyme quantity | μmol |
| $[E]$ | Enzyme concentration | mM |
| $k_{cat}$ | Turnover number | /s |
| $k_{cat}/K_m$ | Specificity constant | /s/M |
| $K_m$ | Michaelis–Menten constant | mM |
| $P$ | Pressure | bar |
| $P$ | Product quantity | μmol |
| $[P]$ | Product concentration | mM |
| $P^*$ | Product fraction $([S_0]-[S_t])/[S_0]$ | – |
| $R$ | Reaction capacity | mol/s |
| $R_D$ | Viscous resistance | $/m^2$ |
| SC | Cell difference score | – |
| $[S_0]$ | Initial substrate concentration | mM |
| $[S_t]$ | Outflow substrate concentration | mM |
| $T$ | Temperature | °C |
| $t$ | Time | s, min |
| $U_B$ | Specific activity | μmol/g/min |
| $U_V$ | Volumetric productivity | g/L/h |
| $V_s$ | Reaction chamber volume | μL |
| $V_v$ | Void chamber volume | μL |
| $Q$ | Flow rate | μL/min |
| $\beta$ | Voidity $(V_v/V_s)$ | – |
| $\varepsilon$ | Molar extinction coefficient | /M/cm |
| $\lambda$ | Wavelength | nm |
| $v$ | Reaction velocity | nmol/min |
| $\Pi$ | Plan view image of the chip | – |

## References

1. Poppe, L.; Paizs, C.; Kovács, K.; Irimie, F. D.; Vértessy, B. G. *Meth. Mol. Biol*. **2012**, *794*, 3–19.
2. Hodgins, D.S. *J. Biol. Chem*. **1971**, *246*, 2977–2985.
3. Sarkissian, C. N.; Gámez, A. *Mol. Gen. Metab*. **2005**, *86*, 22–26.
4. Hughes, A. Amino Acids, Peptides and Proteins in Organic Chemistry Volume 1; Weinheim Germany: Wiley VCH, 2009; p. 94. ISBN 9783527320967.
5. Munirathinam, R.; Huskens, J.; Verboom, W. *Adv. Synth. Catal*. **2015**, *357*, 1093–1123.
6. Sheng, J.; Zhang, L.; Lei, J.; Ju, H. *Anal. Chim. Acta* **2012**, *709*, 41–46.
7. Wang, M. S.; Black, J. C.; Knowles, M. K.; Reed, S. M. *Anal. Bioanal. Chem*. **2011**, *401*, 1309–1318.
8. Song, Y. S.; Shin, H. Y.; Lee, J. Y.; Park, C.; Kim, S. W. *Food Chem*. **2012**, *133*, 611–617.
9. He, P.; Greenway, G.; Haswell, S. J. *Microfluid. Nanofluid*. **2010**, *8*, 565–573.
10. Gijs, M. A. M.; Lacharme, F.; Lehmann, U. *Chem. Rev*. **2010**, *110*, 1518–1563.
11. Weiser, D.; Bencze, L. C.; Bánóczi, G.; Ender, F.; Kókai, E.; Szilágyi, A.; Vértessy, B. G.; Farkas, Ö; Paizs, C.; Poppe, L. *ChemBioChem* **2015**, *16*, 2283–2288.
12. Ender, F.; Weiser, D.; Vitéz, A.; Sallai, G.; Németh, M.; Poppe, L. *Microsyst. Technol*. [First online: 14 December 2015] DOI 10.1007/s00542-015-2749-3.
13. ANSYS Fluent, ANSYS Ver 16.0 (ANSYS Inc. Canonsburg, USA).
14. Lilly, M. D.; Hornby, W. E.; Crook, E. M. *Biochem. J*. **1966**, *100*, 718–723.
15. Paizs, C.; Katona, A.; Rétey, J. *Chem. Eur. J*. **2006**, *12*, 2739–2744.
16. Gloge, A.; Zoń, J.; Kővári, Á.; Poppe, L.; Rétey, J. *Chem. Eur. J*. **2000**, *6*, 3386–3390.
17. Bradford, M. M. *Anal. Biochem*. **1976**, *72*, 248–254.